

Analysis of Arrhenius activation energy on magnetohydrodynamic gyrotactic microorganism flow through porous medium over an inclined stretching sheet with thermophoresis and Brownian motion

Proc IMechE Part E:

J Process Mechanical Engineering

1–15

© IMechE 2022

Article reuse guidelines:

sagepub.com/journals-permissions

DOI: 10.1177/09544089221128768

journals.sagepub.com/home/pie



Bhupendra Kumar Sharma¹ , Umesh Khanduri¹,
Nidhish K Mishra² and Ali J Chamkha³

Abstract

This paper aims to examine the combined effects of Arrhenius activation and microorganisms on unsteady flow through a porous medium with thermophoresis and Brownian motion over an inclined stretching sheet. The governing partial differential equations are transformed into a set of non-linear ordinary differential equations using similarity analysis. The resultant non-linear coupled ordinary differential equations are solved numerically using the boundary value problem solver in MATLAB. The effects of the physical parameter such as magnetic field parameter (M), thermal radiation parameter (R), permeability parameter (K), Eckert number (Ec), thermophoresis parameter (N_t) and Brownian motion parameter (N_b) on the velocity, temperature, concentration profiles, skin friction coefficient, Nusselt number, and the local Sherwood number are presented and analysed graphically. The comparison has been made with previously published work, and there is a good agreement. These results may be helpful in geothermal engineering, energy conversation and disposal of nuclear waste material. Furthermore, scientists can employ this technique in medical fields such as gene therapy and the synthesis of drug delivery systems.

Keywords

Magnetohydrodynamic, Arrhenius activation energy, thermophoresis and Brownian motion, porous medium, chemical reaction

Date received: 27 April 2022; accepted: 7 September 2022

Introduction

The study of a viscous, incompressible fluid with heat transfer over a stretching sheet has grown enormously due to its vast application in industrial fields such as polymer extrusion, glass blowing, electronic chips, and spinning fibres. Crane¹ was the first to investigate and report the fluid flow due to the stretching of the flat surface. He considered the boundary layer flow over steady, incompressible fluid that moves due to the stretching of a flat sheet. This study is essential as Crane obtained the exact solution of the two-dimensional Navier–Stokes equations. Gupta and Gupta² investigated the flow over the flat stretching sheet considering suction and blowing effects and neglecting the viscous dissipation. Ali³ further extended the study of stretching surface with power-law velocity and temperature variations for several values of injection parameters. Cortell⁴ investigated the fluid flow over a linearly stretching surface and obtained the analytic solutions for this kind

of flow with suction and blowing. For an engineering application, the variable thickness is more related to the physical problem than a thin flat plate. In the above-mentioned studies, researchers only deal with a steady flow. But, Ishak et al.⁵ and Bhattacharyya⁶ have analysed the unsteady flow influenced by the stretching sheet making it nearer to the circumstance in practical application.

¹Department of Mathematics, Birla Institute of Technology and Science, Pilani, Rajasthan, India

²Department of Basic Sciences, College of Sciences and Theoretical Studies Saudi Electronic University, Riyadh, Saudi Arabia

³Faculty of Engineering, Kuwait College of Science and Technology, Doha District, Safat, Kuwait

Corresponding author:

Bhupendra Kumar Sharma, Department of Mathematics, Birla Institute of Technology and Science, Pilani, Rajasthan, India.

Email: bhupen_1402@yahoo.co.in

Magnetohydrodynamics (MHD) is currently going through a period of significant expansion and differentiation. Moving fluid interaction with magnetic field makes the study of the topic of MHD fluid highly essential due to its application in electrochemistry, chemical engineering, geophysics, astrophysics, in electric power generation, purification of crude oil, glass manufacturing, processing of food-stuffs, paper production, etc. Sheikholeslami et al.⁷ studied the effects of MHD on free convection of nanofluids. Further, Kolsi et al.⁸ employed the Keller box methodology to study the hybrid nanofluid over the stretching cylinder with stagnation point flow. Sharma et al.⁹ studied the effects of viscous dissipation, radiation, and magnetic field on the MHD slip flow of hybrid nanoparticles. According to their research, the volumetric flow rate increases as velocity slips and the viscosity parameter increases. Several other researchers^{10–14} studied the effect of heat and mass transfer on the MHD flow.

Thermophoresis is a process in which suspended particles migrate from higher to lower regions due to temperature gradient. Its application can be seen in nuclear power plants, in micro contamination, in the aerosol collector. The aerosol is the suspended particles or water droplets present in the air. The force that moves these aerosol particles due to temperature gradient is known as the thermophoretic force. A typical example of this phenomenon is the blackening of the glass globe of kerosene lantern; the carbon particles get deposited on the glass globe due to the temperature gradient generated between the flame and glass globe. A theoretical model of aerosol particle deposition by thermophoretic force over a stretching sheet examined by Huang et al.¹⁵ Bai et al.¹⁶ perceived the effects of Brownian motion and thermophoresis on MHD Maxwell nanofluids past a stretching sheet. Sharma et al.¹⁷ evaluated MHD blood flow via a stenosed artery with the Soret and Dufour effect in the presence of heat radiation. Their research found that increasing thermal radiation absorption in patients receiving thermal radiation therapy reduces resistance to blood flow caused by magnetic fields and stenosis.

Viscous dissipation is an irreversible mechanism in which fluid gets heated by taking energy from the movement of the fluid and transforming it into the fluid's internal energy. Yazdi et al.¹⁸ numerically investigated the effect of viscous dissipation with convective boundary on the MHD flow past through a horizontal sheet. Das et al.¹⁹ examined the effects of viscous dissipation and joule heating on MHD flow. Haile et al.²⁰ employed the Keller box methodology to investigate the impact of viscous dissipation on MHD flow numerically. Mishra et al.²¹ considered the MHD flow in a rotating channel with the hall effect. They examined the influence of pertinent parameters like Hartmann number, suction parameter, and rotation parameter. Tripathi et al.²² analysed the two-phase blood flow on stenosis artery with variable viscosity and joule heating. The inner layer has variable viscosity in this two-phase flow, while the core region viscosity depends on the hematocrit level.

The chemical reaction can be classified as either homogeneous or heterogeneous. This classification is determined by whether the reaction takes place in a single phase or at the surface. Anjalidevi and Kandasamy²³ used the numerical technique to analysed the flow along with the semi-infinite plate and studied the effect of a chemical reaction and species concentration. Afify²⁴ reviewed an elastic sheet immersed in the porous medium and studied chemically reactive species' diffusion. Reddy et al.²⁵ analyse the effect of chemical reaction on MHD flow past through an inclined stretching sheet. Several other researchers^{26–33} studied the effect of chemical reaction on the various types of flow past through the stretching sheet.

Activation energy is the minimum energy required to function atoms or molecules to flinch a chemical reaction. Initially, it was considered that the reaction rates had a significant temperature dependency. Later, it was discovered that kinetic studies were more focused on assessing the influence of reactant concentrations than temperature. Arrhenius proposed the theory of electrolytic dissociation, and his kinetic studies included the electrolyte and measurements of the effects of neutral salts. The modified Arrhenius law^{34,35} (IUPAC Goldbook definition of modified Arrhenius equation) is usually of the form $K_r^2(\tilde{C} - \tilde{C}_\infty) \exp\left(\frac{-E_a}{\tilde{k}T}\right)\left(\frac{\tilde{T}}{\tilde{T}_\infty}\right)^n$, where E_a is the activation energy, \tilde{k} is the Boltzmann constant, n is the rate of fitting constant that lies between $(-1,1)$, and K_r^2 is a constant chemical reaction. Bestman³⁶ studied the effect of natural convection and suction in a porous medium by incorporating Arrhenius activation energy with binary chemical reactions. Zeeshan et al.³⁷ analysed the impact of activation energy by considering the analytic method (HAM) on Couette-Poiseuille flow, while Khan et al.³⁸ discussed the entropy generation in MHD flow with the combined effect of a chemical reaction and Arrhenius activation energy. Further, Khan et al.³⁹ examined the MHD flow of titanium alloy nanoparticles with activation energy and binary chemical reaction. Motile microorganisms generally flow upward due to the influence of magnetic field stimuli, gravity, chemical concentration, and light. The presence of algae and bacteria in a base fluid produces the process of bioconvection. Xu and pop⁴⁰ studied the mixed convection flow of nanoparticles and gyrotactic microorganisms by assuming that the suspended nanoparticles are in a diluted state. Naz et al.⁴¹ studied the MHD flow of Williamson fluid over a stretching cylinder for the Newtonian and non-newtonian cases. Mansour et al.⁴² numerically investigated the MHD mixed convection flow and inclination effect passed through the square-filled cavity with gyrotactic microorganisms. In the manufacturing industry, mineral oil is used as cutting fluids for machinery. Depletion of mineral oil is driving the industries to search for new renewable raw materials. D'Addona et al.⁴³ explored this new renewable source by using microorganisms as a lubricant component in cutting fields. Several other researchers^{44–47} studied the suspension of gyrotactic microorganisms and analysed the natural bio-convection boundary layer nanofluids.

In recent years, the study of porous media has attained much attention due to its application in the solidification process, nuclear fuel debris treatment, recovery of crude oil from reservoir rocks. Meanwhile, due to the applications of MHD fluid in many systems, the researchers are investigating the combined effect of MHD flow and heat transfer in porous media. Kolsi et al.⁴⁸ studied the convective hybrid nanofluid with a partial porous layer and assessed the impact of the rotating cylinder. Krishna et al.⁴⁹ advanced the study by including the MHD second-grade fluid through the porous medium over a stretching sheet. Nandkeolyar et al.⁵⁰ considered the MHD three-dimensional (3D) Casson fluid with Hall and radiation effect through the porous medium. El-dabe and Mostapha et al.⁵¹ studied the Walter-B fluid with thrombosis by employing the 'regular perturbation method' by considering the assumption of long wavelength and low Reynold number. Krishna et al.⁵² obtained the analytic solution for unsteady MHD flow over the vertical surface using the Laplace transformation. They observed the increasing trend in the velocity profile for permeability parameter (K). Zaib et al.⁵³ discussed the effect of thermal and velocity slip parameters on the Casson fluid over the vertical plate and observed the unique solution for assisting flow whereas dual solution for opposing flow. Sangeetha et al.⁵⁴ examined the influence of viscous dissipation and ohmic heating on nanofluid flow embedded in a porous non-Darcian medium. Their research discovered that the inertia coefficient and the porosity parameter had a reducing effect on the velocity profile. Further, Sharma et al.⁵⁵ studied the effect of unsteady Couette flow through porous medium.

In the present study, we have analysed the effect of Arrhenius activation and microorganisms on unsteady flow through porous medium. The flow is subjected to uniform inclined magnetic field. Highly non-linear momentum, energy, and concentration equations are solved numerically using Matlab 'Bvp4c' solver package. The combined effect of physical parameters may be helpful to scientists to perceive their results. The present problem can help scientists to employ this technique in building the metallic sheet around the thermonuclear fusion-fission hybrid reactor, processing the liquid metal from the mushy zone by solidification, and in medical fields such as gene therapy and synthesizing of drug delivery systems.

The novelty of the present work is:

- The combined effects of Arrhenius activation and microorganisms on unsteady flow through a porous medium have been studied with thermophoresis and Brownian motion over an inclined stretching sheet.
- The uniform inclined magnetic field, Joule heating, viscous dissipation and radiation are considered.

Mathematical formulation

Consider an unsteady, incompressible, two-dimensional MHD flow over a stretching sheet, as shown in

Figure 1. The time-dependent permeable sheet inclined at an angle α to vertical has been considered. The sheet is initially at rest and starts to move along the x -axis with velocity $\tilde{U}_w^*(x, t) = \frac{ax}{(1-bt)}$. The surface has variable temperature is \tilde{T}_w^* and variable concentration \tilde{C}_w^* , whereas the ambient temperature \tilde{T}_∞ and ambient concentration of the fluid is \tilde{C}_∞ . A uniform magnetic field is applied perpendicular to the sheet, with an acute angle ξ . The induced magnetic field is negligible as the magnetic Reynold number is less than unity.

Assuming the fluid properties to be constant and using Boussinesq approximation (see the literary works^{6,25}), the continuity, momentum, energy, concentration equations, and micro-organisms (see the literary works^{56,57}) are:

Continuity:

$$\frac{\partial \tilde{u}_\tau}{\partial x} + \frac{\partial \tilde{v}_\tau}{\partial y} = 0, \quad (1)$$

Momentum:

$$\begin{aligned} \frac{\partial \tilde{u}_\tau}{\partial t} + \tilde{u}_\tau \frac{\partial \tilde{u}_\tau}{\partial x} + \tilde{v}_\tau \frac{\partial \tilde{u}_\tau}{\partial y} = & g\beta(\tilde{T} - \tilde{T}_\infty) \cos \alpha - g\lambda(\tilde{N} - \tilde{N}_\infty) \\ & \cos \alpha + g\beta^*(\tilde{C} - \tilde{C}_\infty) \cos \alpha \\ & + \nu \frac{\partial^2 \tilde{u}_\tau}{\partial y^2} - \frac{\sigma B^2(t)}{\rho} \sin^2 \xi \tilde{u}_\tau \\ & - \frac{\nu}{l_1(t)} \tilde{u}_\tau, \end{aligned} \quad (2)$$

Energy:

$$\begin{aligned} \frac{\partial \tilde{T}}{\partial t} + \tilde{u}_\tau \frac{\partial \tilde{T}}{\partial x} + \tilde{v}_\tau \frac{\partial \tilde{T}}{\partial y} = & \frac{\kappa}{\rho C_p^*} \frac{\partial^2 \tilde{T}}{\partial y^2} - \frac{1}{\rho C_p^*} \frac{\partial q_r}{\partial y} + \frac{\nu}{C_p^*} \left(\frac{\partial \tilde{u}_\tau}{\partial y} \right)^2 \\ & + \zeta \frac{D_\tau^*}{\tilde{T}_\infty} \left(\frac{\partial \tilde{T}}{\partial y} \right)^2 + \frac{\sigma B^2(t)}{\rho C_p^*} \sin^2 \xi \tilde{u}_\tau^2 \\ & + \zeta D_B^* \frac{\partial \tilde{C}}{\partial y} \frac{\partial \tilde{T}}{\partial y}, \end{aligned} \quad (3)$$

Concentration:

$$\begin{aligned} \frac{\partial \tilde{C}}{\partial t} + \tilde{u}_\tau \frac{\partial \tilde{C}}{\partial x} + \tilde{v}_\tau \frac{\partial \tilde{C}}{\partial y} = & D_B^* \frac{\partial^2 \tilde{C}}{\partial y^2} + \frac{D_\tau^*}{\tilde{T}_\infty} \left(\frac{\partial^2 \tilde{T}}{\partial y^2} \right) \\ & - K_r^2 (\tilde{C} - \tilde{C}_\infty) \exp\left(\frac{-E_a}{\tilde{\kappa} \tilde{T}}\right) \\ & \times \left(\frac{\tilde{T}}{\tilde{T}_\infty} \right)^n, \end{aligned} \quad (4)$$

Micro-organisms:

$$\begin{aligned} \frac{\partial \tilde{N}}{\partial t} + \tilde{u}_\tau \frac{\partial \tilde{N}}{\partial x} + \tilde{v}_\tau \frac{\partial \tilde{N}}{\partial y} = & D_n \frac{\partial^2 \tilde{N}}{\partial y^2} \\ & - \frac{\partial}{\partial y} \left(\tilde{N} \frac{\tilde{b}_w}{\tilde{C} - \tilde{C}_\infty} \frac{\partial \tilde{C}}{\partial y} \right). \end{aligned} \quad (5)$$

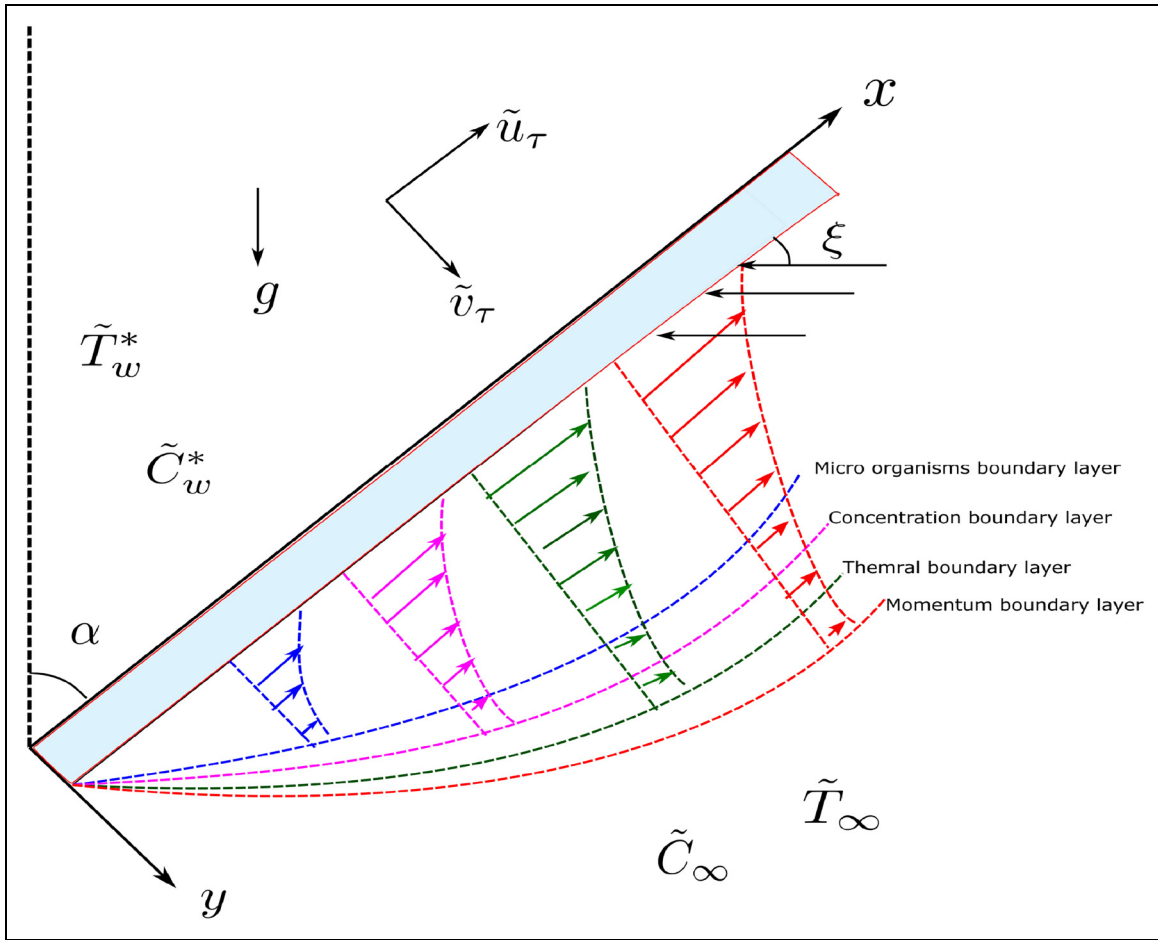


Figure 1. Physical sketch of the fluid flow through an inclined stretching sheet.

The associate boundary condntions are as follows:

$$\begin{cases} \tilde{u}_\tau = \tilde{U}_w^* + H\mu \frac{\partial \tilde{u}_\tau}{\partial y}, \tilde{v}_\tau = \tilde{V}_w^*, \tilde{T} = \tilde{T}_w^* + P \frac{\partial \tilde{T}}{\partial y}, \\ \tilde{C} = \tilde{C}_w^* + J \frac{\partial \tilde{C}}{\partial y}, \tilde{N} = \tilde{N}_w^* + L \frac{\partial \tilde{N}}{\partial y} & \text{at } \bar{y} = 0 \\ \tilde{u}_\tau \rightarrow 0, \tilde{T} \rightarrow \tilde{T}_\infty, \tilde{C} \rightarrow \tilde{C}_\infty, \tilde{N} \rightarrow \tilde{N}_\infty & \text{as } \bar{y} \rightarrow \infty. \end{cases} \quad (6)$$

where, $H = H_0(1 - bt)^{\frac{1}{2}}$ represent the velocity slip factor, $P = P_0(1 - bt)^{\frac{1}{2}}$ represent the thermal slip factor, $J = J_0(1 - bt)^{\frac{1}{2}}$ represent the concentration slip factor, and $L = L_0(1 - bt)^{\frac{1}{2}}$ represent the microorganisms slip factor. The stretching velocity $\tilde{U}_w^*(x, t)$, surface temperature $\tilde{T}_w^*(x, t)$, the concentration $\tilde{C}_w^*(x, t)$ and the microorganisms $\tilde{N}_w^*(x, t)$ are given as (see Ishak et al.⁵):

$$\begin{aligned} \tilde{U}_w^* &= \frac{ax}{1-bt}, \\ \tilde{T}_w^* &= \tilde{T}_\infty + \frac{dx}{1-bt}, \\ \tilde{C}_w^* &= \tilde{C}_\infty + \frac{cx}{1-bt}, \\ \tilde{N}_w^* &= \tilde{N}_\infty + \frac{ex}{1-bt}. \end{aligned} \quad (7)$$

where, a, d, c, b and e are constant and satisfies the condition $d, b, c, e \geq 0, a > 0$, and $bt < 1$. In equation (6),

\tilde{V}_w^* represent the injection/suction velocity:

$$\tilde{V}_w^* = -\sqrt{\frac{\nu \tilde{U}_w^*}{x}} f(0). \quad (8)$$

Here \tilde{V}_w^* represent the velocity of mass trasfer at the surface with $\tilde{V}_w^* > 0$ represents injection and $\tilde{V}_w^* < 0$ represents the suction case. The expression $l_1(t)$ used in the equation (2) represents the time-dependent permeability and it satisfies the equation $l_1(t) = l_2(1 - bt)$. Let us now consider the magnetic field $B(t) = B_0(1 - bt)^{-\frac{1}{2}}$ and chemical reaction parameter as $K_r^2(t) = \Gamma_0(1 - bt)^{-1}$. Here B_0 represents the magnetic field at initial time, and Γ_0 as constant.

In equation (3), the radiative heat flux is approximated by Rosseland mean approximation and it is simplified as (also see Refs.^{26,29}):

$$q_r = -\frac{4\sigma^*}{3k^*} \frac{\partial \tilde{T}^4}{\partial y}. \quad (9)$$

Here σ^* and k^* are the Stefan-Boltzman constant and the mean absorption coefficient, respectively. We assume the temperature difference within the flow is sufficiently small. So, linearlizing the term \tilde{T}^4 using taylor series

about free steam function \tilde{T}_∞ , and neglecting higher order terms:

$$\tilde{T}^4 \cong 4\tilde{T}\tilde{T}_\infty^3 - 3\tilde{T}_\infty^4. \quad (10)$$

Now, introducing similarity transformations (see literary works^{5,38}):

$$\begin{cases} \eta = a^{\frac{1}{2}}\nu^{-\frac{1}{2}}(1 - bt)^{-\frac{1}{2}}y, \\ \psi = a^{\frac{1}{2}}x\nu^{\frac{1}{2}}(1 - bt)^{-\frac{1}{2}}f(\eta), \\ \theta(\eta) = \left(\frac{\tilde{T} - \tilde{T}_\infty}{\tilde{T}_w^* - \tilde{T}_\infty}\right), \\ \phi(\eta) = \left(\frac{\tilde{C} - \tilde{C}_\infty}{\tilde{C}_w^* - \tilde{C}_\infty}\right), \\ \chi(\eta) = \left(\frac{\tilde{N} - \tilde{N}_\infty}{\tilde{N}_w^* - \tilde{N}_\infty}\right). \end{cases} \quad (11)$$

where, η is the independent similarity variable, ψ represents the stream function and it is defined as $\tilde{u}_\tau = \frac{\partial\psi}{\partial y}$, $\tilde{v}_\tau = -\frac{\partial\psi}{\partial x}$, which identically satisfies equation (1). Now, substitute equations (10) and (11) into equations (2)–(5), to get differential equations as follows:

$$\begin{aligned} f'''' + ff'' - A\left(f' + \frac{1}{2}\eta f'''\right) - (f')^2 + Gr\theta \cos \alpha \\ + Gc\phi \cos \alpha - Rb\chi \cos \alpha - M^2 f' \sin^2 \xi - \frac{1}{K} f' \\ = 0, \end{aligned} \quad (12)$$

$$\begin{aligned} \frac{(1+R)}{Pr}\theta'' + f\theta' - f'\theta - A\left(\theta + \frac{1}{2}\eta\theta'\right) \\ + Ec(f'')^2 + Ec * M^2 (f')^2 \sin^2 \xi + N_b\theta'\phi' \\ + N_t(\theta')^2 \\ = 0, \end{aligned} \quad (13)$$

$$\begin{aligned} \frac{1}{Sc}\phi'' + f\phi' - f'\phi - A\left(\phi + \frac{1}{2}\eta\phi'\right) - \gamma\phi \\ + \left(\frac{N_t}{N_b Sc}\right)\theta'' - \gamma(1 + \theta\delta)^n \exp\left(\frac{-E}{1 + \theta\delta}\right) \\ = 0, \end{aligned} \quad (14)$$

$$\begin{aligned} \chi'' - Pe(\zeta + \chi)\phi'' - Pe\chi'\phi' \\ - Sb\left(\frac{A}{2}\eta\chi' + A\chi + \chi f' - \chi'f\right) \\ = 0. \end{aligned} \quad (15)$$

The associated boundary conditions are as follows:

$$\begin{cases} f = S, \quad f' = 1 + S_f f''(0), \quad \theta = 1 + S_t \theta'(0), \\ \phi = 1 + S_c \phi'(0), \quad \chi = 1 + S_n \chi'(0) & \text{at } \eta = 0, \\ f' \rightarrow 0, \quad \theta \rightarrow 0, \quad \phi \rightarrow 0, \quad \chi \rightarrow 0 & \text{as } \eta \rightarrow \infty. \end{cases} \quad (16)$$

The dimensionless velocity slip S_f , thermal slip S_t , solutal slip S_c and micro-organisms slip S_n are defined as follows:

$$S_f = H_0 \rho \sqrt{av}, \quad S_t = P_0 \sqrt{\frac{a}{\nu}}, \quad S_c = J_0 \sqrt{\frac{a}{\nu}}, \quad S_n = L_0 \sqrt{\frac{a}{\nu}}. \quad (17)$$

Here, prime denotes the differentiation with respect to η . In equations (12)–(15), if $A = 0$, it will correspondence that the problem reduce to the steady state flow. Also, in equation (16), if $S > 0$, it indicates suction, $S < 0$ indicates injection. The dimensionless numbers and parameter used in equations (12)–(15) are specified in Supplemental Table 1.

Quantities of physical interest

The quantities like heat transfer rate, skin friction coefficient, mass transfer and local density number of motile microorganism are defined as follows:

$$\begin{cases} Nu_x = \frac{x(q_w + q_r)}{\kappa(\tilde{T}_w^* - \tilde{T}_\infty)}, \\ C_f = \frac{\tau_w}{\rho \tilde{U}_w^* 2}, \\ Sh_x = \frac{m_w x}{\rho D_B^* (\tilde{C}_w^* - \tilde{C}_\infty)}, \\ Nn_x = \frac{n_w x}{\rho D_n (\tilde{N}_w^* - \tilde{N}_\infty)}. \end{cases} \quad (18)$$

where the surface heat flux, wall shear stress, mass flux, and motile microorganisms flux are given by Ram Reddy et al.⁵⁸:

$$\begin{aligned} q_w = -\kappa \left(\frac{\partial \tilde{T}}{\partial y}\right)_{y=0}, \quad \tau_w = \mu \left(\frac{\partial \tilde{u}_\tau}{\partial y}\right)_{y=0}, \\ m_w = -\rho D_B^* \left(\frac{\partial \tilde{C}}{\partial y}\right)_{y=0}, \quad n_w = -\rho D_n \left(\frac{\partial \tilde{N}}{\partial y}\right)_{y=0}. \end{aligned} \quad (19)$$

Use equation (19), to rewrite quantity (18) as follows:

$$\begin{aligned} Re_x^{-\frac{1}{2}} Nu_x = -(1 + R)\theta'(0), \quad Re_x^{\frac{1}{2}} C_f = 2f''(0), \\ Re_x^{-\frac{1}{2}} Sh_x = -\phi'(0), \quad Re_x^{-\frac{1}{2}} Nn_x = -\chi'(0). \end{aligned} \quad (20)$$

The quantity like Nusselt number Nu_x , skin-friction coefficient C_f , Sherwood number Sh_x and motile microorganism density are dependent on the variation of the factors $-\theta'(0)$, $f''(0)$, $-\phi'(0)$ and $-\chi'(0)$ respectively.

Method of solution

The system of equations (12)–(15) with boundary conditions (16) are solved numerically using BVP4C solver in Matlab. These equations are first converted into a system of the first-order IVP, which gives seven differential equations having seven unknowns. The value of η will

vary from 2 to 30, according to physical parameters. Let us assume that:

$$\begin{cases} h_1 = f, & h_2 = f', & h_3 = f'', \\ h_4 = \theta, & h_5 = \theta', \\ h_6 = \phi, & h_7 = \phi', \\ h'_5 = Y \text{ (Say)}, \\ h_8 = \chi, & h_9 = \chi', \\ h'_9 = \Phi \text{ (Say)}. \end{cases} \quad (21)$$

After employing the above variables in equations (12–15), we get

$$\begin{cases} h'_1 = h_2, \\ h'_2 = h_3, \\ h'_3 = h_2^2 - h_1 h_3 + Ah_2 + 0.5A\eta h_3 - Grh_4 \cos(\alpha) \\ \quad - Gch_6 \cos \alpha + Rbh_8 \cos \alpha + M^2 \sin^2 \xi h_2 + h_2/K, \\ h'_4 = h_5, \\ h'_5 = \frac{Pr}{1+R} [h_2 h_4 - h_1 h_5 + Ah_4 + 0.5A\eta h_5 - Ech_2^2 \\ \quad - M^2 Ech_2^2 \sin^2 \xi - N_b h_5 h_7 - N_t h_5^2], \\ h'_6 = h_7, h'_7 = Sc[h_2 h_6 - h_1 h_7 + Ah_6 + 0.5A\eta h_7 \\ \quad + \gamma \exp\left(\frac{-Ea}{1+h_4}\right) (1 + \delta h_4)^n h_6] - \frac{N_t}{N_b} Y, \\ h'_8 = h_9, \\ h'_9 = Sb[0.5A\eta h_9 + Ah_8 + h_8 h_2 - h_9 h_1] + Pe(\chi + \zeta)\Phi. \end{cases} \quad (22)$$

And, the boundary conditions now become:

$$\begin{cases} h_1(0) = S, & h_2(0) = 1 + S_f h_3(0), & h_2(\infty) = 0, \\ h_4(0) = 1 + S_i h_5(0), & h_4(\infty) = 0, \\ h_6(0) = 1 + S_c h_7(0), & h_6(\infty) = 0, \\ h_8(0) = 1 + S_n h_9(0), & h_8(\infty) = 0. \end{cases} \quad (23)$$

Result and discussion

In this section, the impacts of various pertinent parameters, such as M , Gr , Sc , γ , R , Pr etc., on velocity, concentration, and temperature profile have been studied and presented graphically and in tabular form. Moreover, the specific values of some parameters as shown in table [1] are kept constant throughout the study unless pointed out in the appropriate graphs. Supplemental Figure 1 depicts the flow chart of the mathematical model.

Validation

In this subsection, the results are compared with previously published work. Figure 2(a) and (b) are used for validating the temperature and concentration profiles of present work with the previous study done by Reddy et al.²⁵ Reddy et al. used the shooting method to solve the dimensionless governing equations. Therefore, in this comparison, the shooting method is employed for the work of Anki Reddy et al.,²⁵ and the BVP4C technique is used in the current study, which works on the collocation method. The iterative process will terminate when the error involved is $\leq 10^{-6}$. From these figures, one observes that there is a good agreement between

our study for temperature and concentration with the previous research.

Dimensionless velocity profile

Figure 3 is portrayed to analyse the influence of different pertinent parameters like magnetic field parameter M , thermal Grashof number Gr , permeability parameter K , velocity slip factor S_f , suction parameter S , inclination angle α on the velocity profile. Figure 3(a) depicts the effect of the magnetic field parameter with fluid velocity $f'(\eta)$. In a magnetic field, electrically conducting fluid generates a retarding force, namely Lorentz force. As $M(0, 1, 2, 3)$ increases, the fluid will experience this retarding force, and its velocity decreases to zero with parameter η . The obtained result from the present study for M show a similar trend as observed in the published work (El-dabe and Mostapha et al.⁵¹). Figure 3(b) shows the variation of velocity profiles $f'(\eta)$ versus η for different values of Gr . Grashof number signifies the ratio of the thermal resistive force to viscous force. The fluid attains the maximum velocity near the wall, and then its speed declines smoothly to zero. From the Figure 3(b), it can be observed that the momentum of fluid increases as the parameter Gr increases. From Figure 3(c), it can be concluded that the fluid velocity $f'(\eta)$ increases as the permeability factor $K(0.1, 0.3, 0.5)$ increases. Permeability is the property of a porous medium that allows the fluid to flow through its interconnecting voids. So, if the permeability factor increases, the rate of fluid flow increases. The findings of present study's for parameters Gr and K are in good agreement with the published work of (Krishna et al.⁵²).

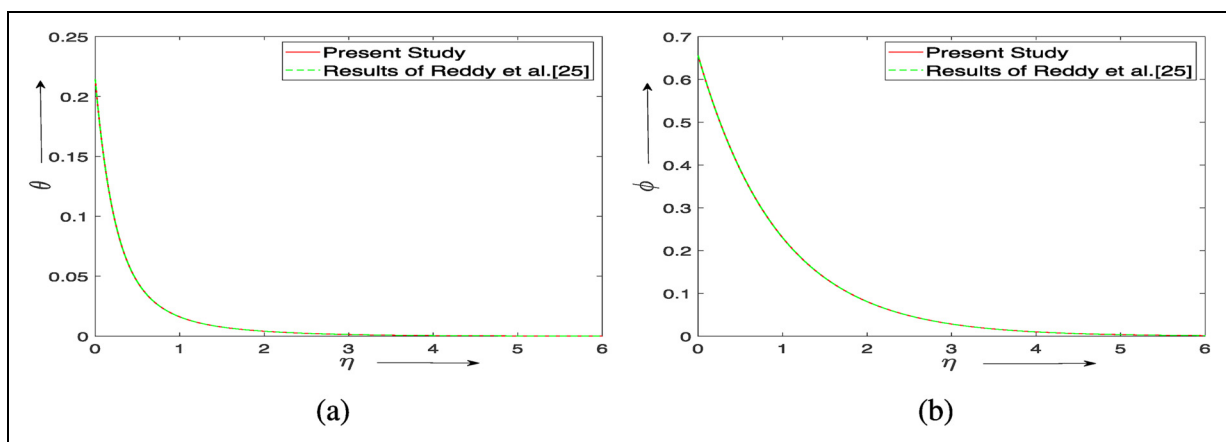
Figure 3(d) depicts the influence of the slip factor on fluid velocity. When slip occurs, fluid velocity will no longer be identical to the stretching wall. The wall transmitted the partial pull to the fluid when the slip condition existed. Thus, the momentum boundary layer decreases with an increase in the slip factor.

The influence of suction on the velocity profile is depicted in Figure 3(e). As suction parameter ($S = 0.5, 1, 1.5$) increases, the fluid velocity decreases due to the retarding force encountered by the fluid. The influence of viscosity causes the fluid to experience high buoyant force resulting in a decline in fluid velocity. In Figure 3(f), an angle $\alpha = 0$ means that the sheet is vertical while an angle $\alpha = \pi/2$ implies that the sheet is horizontal. From the Figure 3(f), it can be seen that there is a decline in the velocity profile if the inclination angle α increases. This reduction in velocity profile happens due to thermal diffusion, which reduces the buoyant force's effect on the fluid. Velocity decreases if the inclination angle increases from 0 to $\pi/4$. But, there is a large reduction in the velocity profile if the inclination angle increases from $\pi/4$ to $\pi/2$. This large variation occurs due to the vanishing of the term $\cos \alpha$ at α equal to $\pi/2$.

In Figure 3(g), an angle $\xi = 0$ means no magnetic field, while an angle $\xi = \pi/2$ implies the transversal

Table 1. Default values of physical parameter used in the work.

Parameters	Values	References	Parameters	Values	References
M	0–5	Bhattacharyya, ⁶ Gandhi et al. ⁵⁹	K	0.1–0.9	Bai et al. ¹⁶
Gr	1–5	Anki Reddy et al. ²⁵	Pr	0.5–1.6	Bai et al., ¹⁶ Tlili et al. ⁴⁵
R	0–5	Bhattacharyya, ⁶ Anki Reddy ²⁵	Ec	0.5–1.6	Bai et al., ¹⁶ Tlili et al., ⁴⁵ Khan et al. ³⁸
N_t	0.1–0.8	Alsaedi et al., ⁴⁴ Tlili et al. ⁴⁵	N_b	0.1–1.3	Alsaedi et al., ⁴⁴ Tlili et al. ⁴⁵
ξ	0– $\pi/2$	Anki Reddy ²⁵	α	0– $\pi/2$	Anki Reddy ²⁵
γ	0.2–4.5	Pal and Mondal ²⁶	Sc	0.5–2.5	Anjalidevi and Kandasamy, ²³ Anki Reddy ²⁵
Pe	0–3	Xu and Pop, ⁴⁰ Kotha et al. ⁴⁶	Sb	0–1.5	Tlili et al., ⁴⁵ Khan et al. ⁴⁷
S_c	0.5–1.5	Anki Reddy ²⁵	S_t	0.5–1.5	Anki Reddy ²⁵
E	0–5	Khan et al. ³⁸	Rb	0.1–2	Alsaedi et al. ⁴⁴
S	0–1.5	Das et al., ¹⁹ Anki Reddy ²⁵	S_f	0–1.5	Das et al., ¹⁹ Anki Reddy ²⁵
δ	0–1.5	Khan et al. ³⁸	A	0–0.5	Anki Reddy et al. ²⁵

**Figure 2.** Comparison graphs for (a) non-dimensional temperature profile for radiation parameter $R = 1.5$, (b) non-dimensional concentration profile for Schmidt Number $Sc = 0.78$.

magnetic field. If the aligned angle ξ increases, $f'(\eta)$ decreases as depicted in the figure. This is the result of the Lorentz force experienced by the fluid. As the aligned angle increases, it causes to strengthen the magnetic field. Figure 3(h) shows the effect of the Rayleigh number on the velocity profile. Increasing the parameter Rb from 0 to 0.2 results in the decrease of fluid velocity by 6.92%, while a 13.52% decline is observed by changing in Rb from 0 to 0.4.

Dimensionless temperature field

Figure 4(a) illustrates the relation between radiation and temperature profile. As the radiation parameter increases, heat produces in the fluid intensifies the thermal boundary layer. This is in good agreement with the published work of Zaib et al.⁵³, which shows the increment in temperature profile for increasing values of radiation parameter R . Figure 4(b) depicts the effect of the Prandtl number on the temperature profile.

Pr is the ratio of the kinematic viscosity to thermal diffusivity, which shows the relative behaviour of momentum and thermal boundary layer. It has been observed that the temperature decreases with an increase in Pr .

For higher values of Pr , the thermal conductivity of the fluid decreases, which results in slower heat diffusion from the heated surface compared to the smaller values of Pr . The results obtained from the present study for Pr show a similar trend as observed in the published work (Krishna et al.⁵²).

The behaviour of the viscous dissipation parameter Ec on temperature profile is shown in Figure 4(c). In our case, $Ec(0.5, 1, 1.5)$ has positive values that signify the fluid heating. This indicates the case $\tilde{T}_w^* > \tilde{T}_\infty$, meaning heat is being supplied across the wall into the fluid. Enhancing the Ec number increases the Joule heating, which adds energy to the fluid boundary layer due to the work done against the drag force. So, the effect of viscous dissipation improves the temperature profile. From Figure 4(d), it can be observed that the increase in the thermal slip causes a reduction in the temperature profile. It happened because less heat is transferred from an extended vessel to the fluid.

Dimensionless concentration field

Figure 5(a) elucidates the effect of chemical reaction parameter on concentration profile. As the chemical reaction

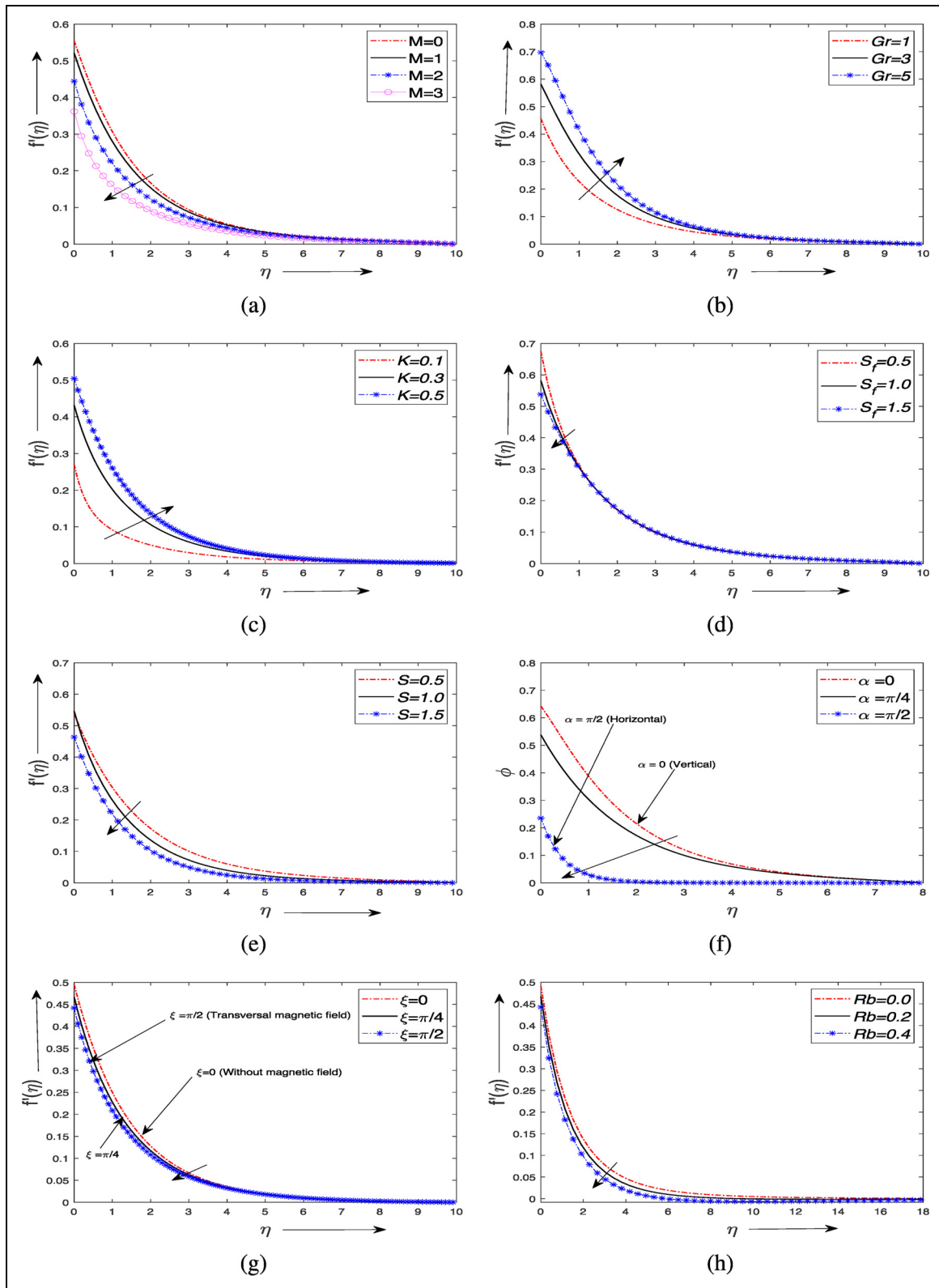


Figure 3. Influence of (a) Magnetic field parameter (M), (b) Grashof Number (Gr), (c) Permeability parameter (K), (d) Slip parameter (S_f), (e) Suction parameter (S), (f) Inclined stretching sheet parameter (α), (g) Inclined magnetic field parameter (ξ), (h) Rayleigh number Rb on velocity profile.

parameter γ increases, it causes the rise in solute molecules and thus, diminishes the concentration boundary layer. Figure 5(b) displays the influence of solutal slip on the concentration profile. It indicates a decline in concentration

profile with an increase in solutal slip. Figure 5(c) demonstrates that the concentration profile decreases by uplifting the Schmidt number. As the value of the Schmidt number ($Sc = 0.57, 0.99, 1.33, 1.50$) increases, it causes a decrease

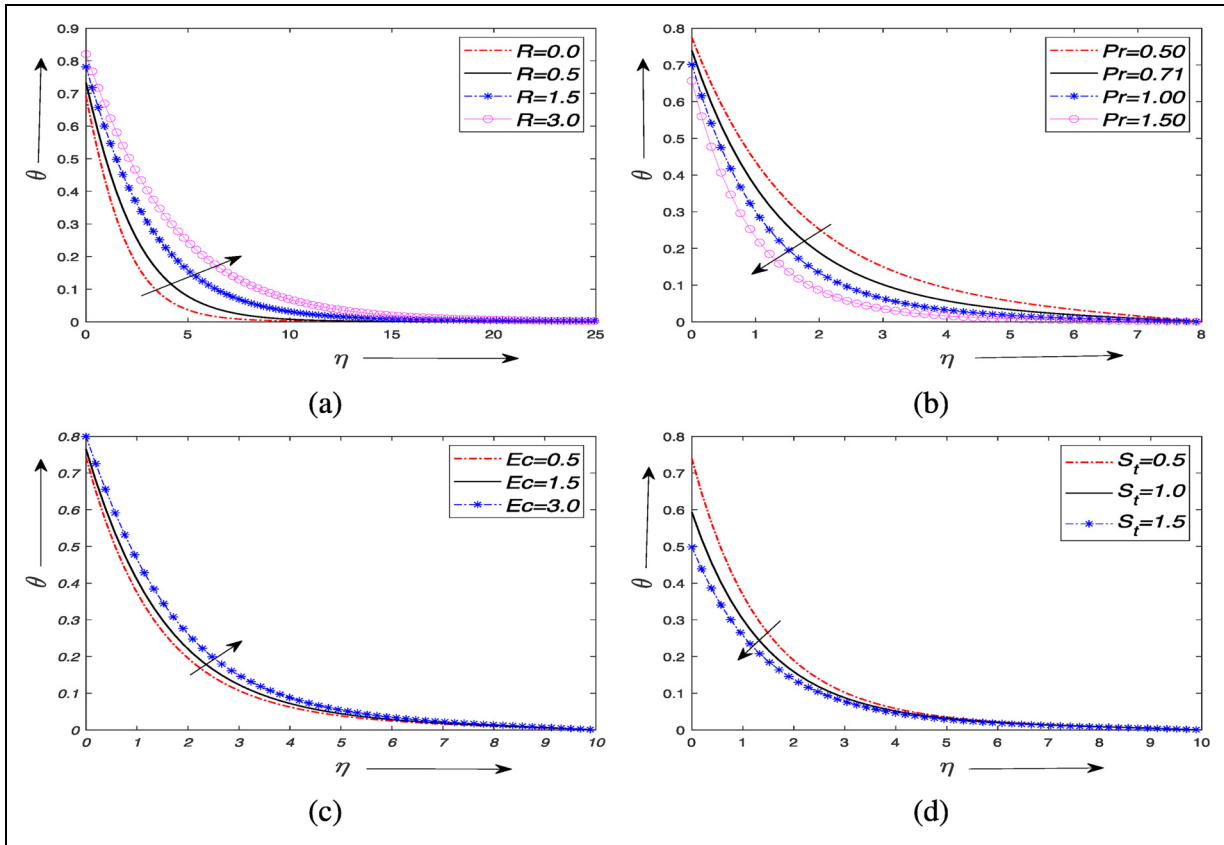


Figure 4. Influence of (a) radiation parameter (R), (b) Prandtl Number Pr , (c) Eckert number Ec , (d) Thermal slip parameter S_t on the temperature profile.

in the diffusion coefficient. Thus, it results in a reduction of the thickness of the solutal boundary layer. Figure 5(d) exhibits the effect of activation energy E on concentration profile. The concentration profile increases with an increase in activation energy. Initially, there is 2.88% increase in concentration profile with an increase in activation energy from $E = 0$ to $E = 0.5$, while 1.39% increase in concentration profile is noted when activation energy increases from $E = 1$ to $E = 1.5$. And, it is noted that the effect of activation energy E becomes negligible on the concentration profile after a certain stage. Figure 5(e) shows that the concentration profile increases with an increase in the thermophoresis parameter. As N_t increases, the thermophoretic force will increase, leading the particle's to move near the wall and thus enhance the concentration boundary layer. It is depicted in Figure 5(f) that the concentration profile decelerated with a rise in the Brownian parameter.

Brownian motion represents the random movement of particles in a zig-zag path. As N_b increases, it enhances the particle's kinetic energy; this results in a rise in temperature profile and moves the particles away from the concentration profile, leading to a decline in the concentration boundary layer.

Dimensionless microorganisms profiles

Figure 6(a) and (b) depict the effect of Sb and Pe on dimensionless microorganisms profile. From the

Figure 6(a), it can be noted that the motile density is the decreasing function of Sb . As the parameter Sb increases from 0.2 to 0.4, the change in motile density is -9.11% , while -6.01% is noted when Sb increases from 0.6 to 0.8. This behaviour shows that there is feeble diffusivity of microorganisms. Figure 6(b) shows the dwindling effect of Pe on motile density.

Peclet number Pe and microorganism's diffusivity are inversely proportional. So, as the Peclet number increases, the microorganism's diffusivity decreases. The findings of current study are in good agreement with the published work of (Ref. ⁵⁴).

Skin-friction coefficient, Nusselt number, Sherwood number and local Nusselt number of motile microorganism

Figure 7(a) and (b) show the influence of Pr on Nusselt number Nu_x & Sherwood number Sh_x . It shows that Nu_x increases with the increase in parameter Pr , but the reverse trend is observed with Sh_x . Figure 7(c) shows that the Sherwood number Sh_x increases with an increase in the Brownian parameter N_b . While Figure 7(d) depicts that Sherwood number Sh_x is a decreasing function of thermophoresis parameter N_t .

Supplemental Table 2 presents the numerical result for skin friction, Nusselt number, Sherwood number and local density number of motile microorganism for

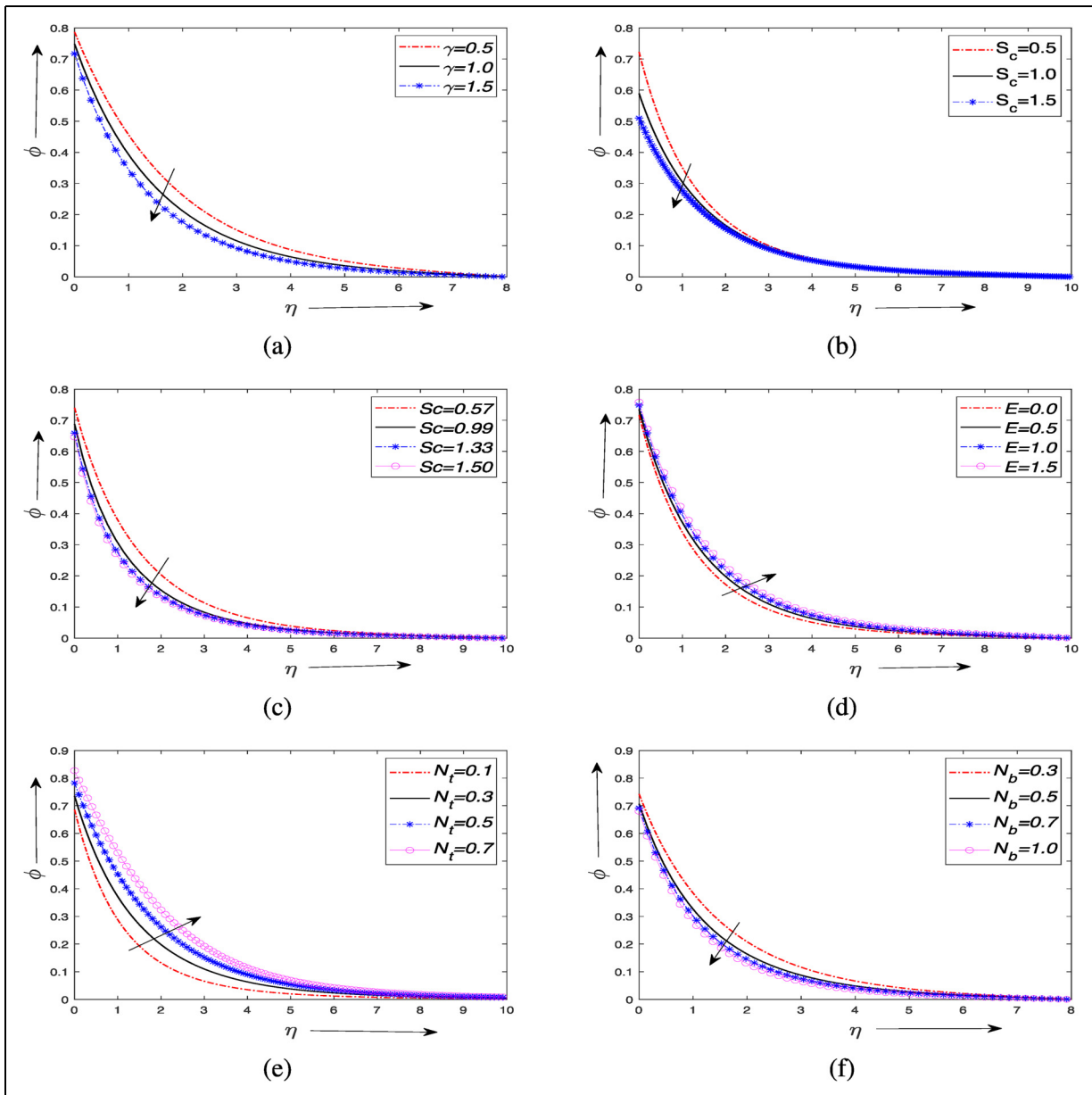


Figure 5. Effect of (a) chemical reaction parameter (γ), (b) Solutal slip parameter (S_c), (c) Schmidt number (Sc), (d) Activation energy E , (e) Thermophoresis parameter (N_t), (f) Brownian motion parameter (N_b), on Concentration profile.

unsteady flow, i.e. $A = 0.5$. Supplemental Table 2 shows that the Nusselt number increases with an increase in parameter Gr , Gc , Pr , E , Pe , Sb while the decreasing trend is observed for parameters M , Ec and R . The Sherwood number increases with the parameters Ec , Pe , Sb , Gr , Gc and R but decreases with Pr and M . Skin friction and Local nusselt number of motile microorganisms decrease with parameter M while a reverse trend is observed for other parameters.

Figures (8 and 9) depict the surface plot to show the effect of different parameters on non dimensional velocity, temperature, concentration and motile density field. Figure 8(a) shows the 3D surface plot of motile density with unsteady parameter A . The motile density decreases with an increase in parameter A . For the change of flow from steady ($A = 0$) to unsteady flow

($A = 2$), there is a 5.48% decrease in motile density. Figure 8(b) and (c) display the temperature and concentration profile with unsteady parameter A and axial direction η . From both the figure, it can be concluded that both the parameter A and η have dwindling effects on temperature and concentration profile, respectively.

Figure 9(a) is drawn to show the effect of activation energy and η on motile microorganism profile. For a fixed value of $\eta = 0$, the microorganism profile increases by 5.93% if activation energy increases from 0 to 2. From Figure 9(b), it can be concluded that the motile density decreases with an increase in parameter Pe . The motile density is higher for smaller values of Pe number, and it decreases with an increase in axial direction η . Figure 9(c) displays the 3D surface plot for motile density with η and Sb . It shows a 52.03% decrease in

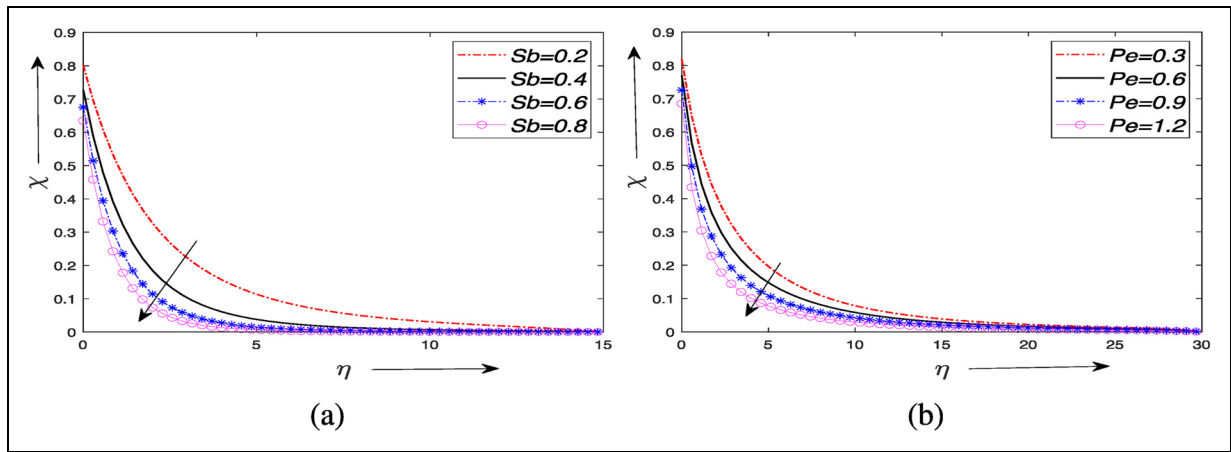


Figure 6. (a) Response of $\chi(\eta)$ versus varied estimates of Bioconvection Lewis number Sb , (b) response of $\chi(\eta)$ versus varied estimates of Peclet number Pe .

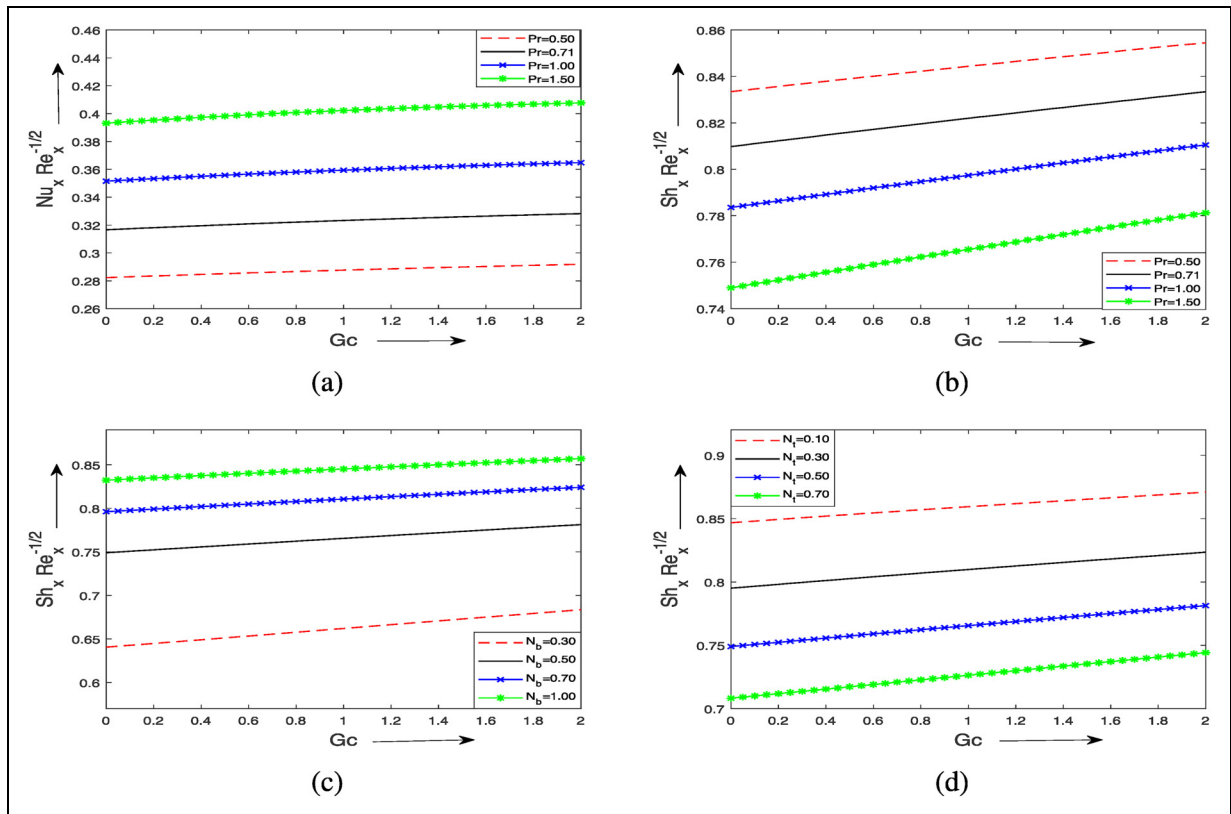


Figure 7. Effect of (a) Prandtl number Pr on Nusselt number and solutal Grashof number Gc , (b) Prandtl number Pr on Sherwood number and solutal Grashof number Gc , (c) Brownian parameter N_b on Sherwood number and solutal Grashof number Gc , (d) Thermophoresis parameter N_t on Sherwood number and solutal Grashof number Gc .

motile density if the parameter Sb increases from one half of the plane $[0,1]$ to another half of the plane $[1,2]$.

Conclusion

In this study, the effects of thermophoresis and Brownian motion on MHD Newtonian fluid containing microorganisms over an inclined stretching sheet through a porous medium with radiation and Arrhenius activation energy

are studied numerically using BVP4C. The governing equations (momentum, continuity, concentration, energy, and micro-organisms equation) are transformed into ordinary differential equations with the help of a similarity transformation. The results are summarized below as:

- Due to the Lorentz force, fluid experiences a retarding force, resulting in a decrement in the velocity profile.

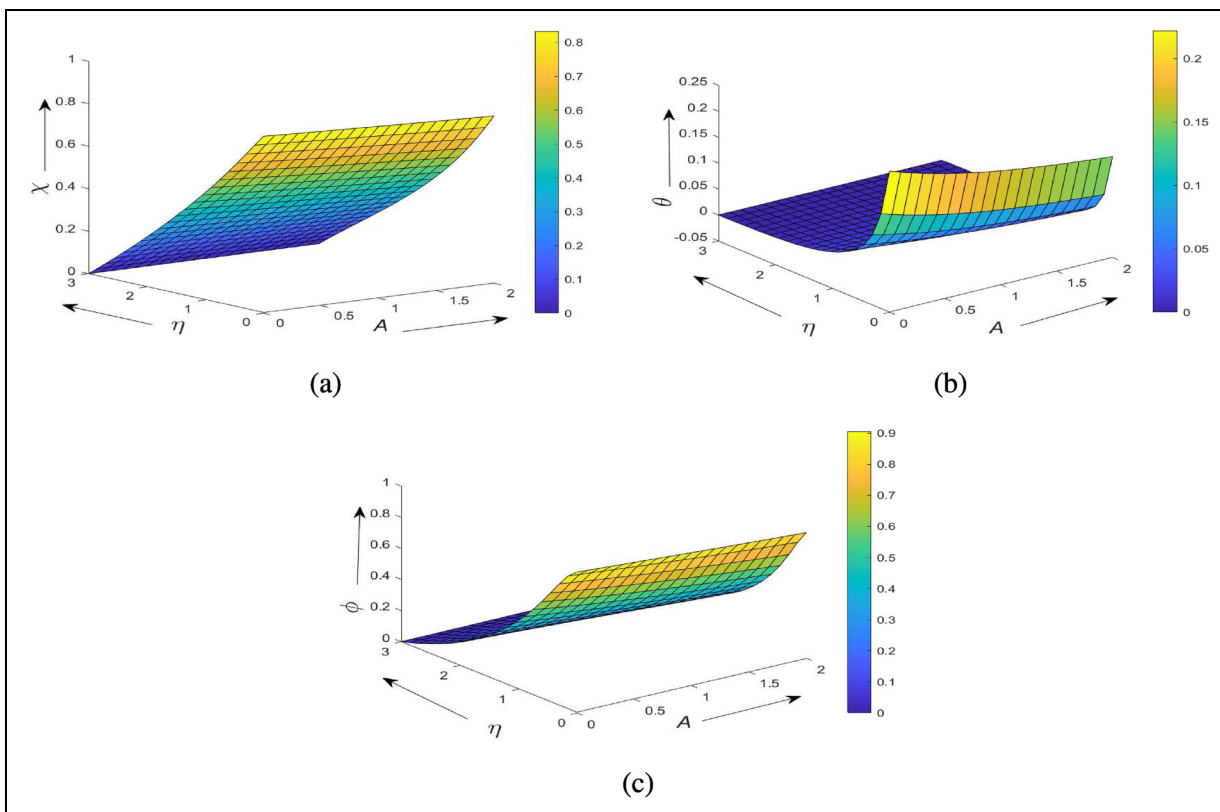


Figure 8. Surface Plot of non-dimensional (a) motile micro-organisms, (b) temperature, (c) concentration by varying axial direction η and unsteadiness parameter A .

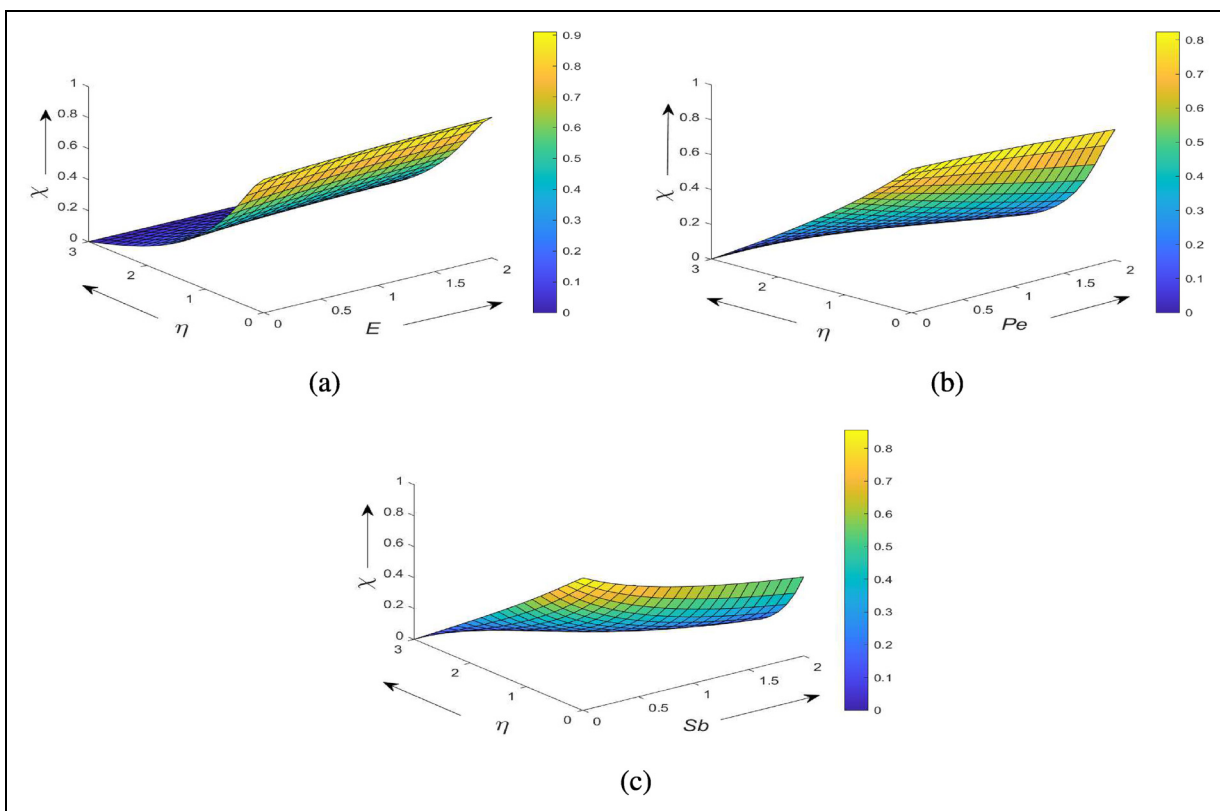


Figure 9. Surface Plot of non-dimensional motile micro-organisms by varying axial direction η and (a) Activation energy E , (b) Peclet number Pe , (c) Bioconvection Lewis number Sb .

- The fluid temperature rises with an increment in Eckert number Ec . This happened due to increased kinetic energy, which leads to collision and heat is dissipated, causing an increase in the thermal boundary layer.
- The concentration profile rises with an increase in the thermophoresis parameter N_t . The higher value of N_t leads the particles to move in the reverse direction of the concentration gradient. Due to this non-uniform distribution, the concentration profile increases.
- The concentration profile decreases with an increment in Brownian motion parameter N_b . Due to this force, the movement of molecules is in the reverse direction, leading to fluid more homogenous.
- The motile density of microorganisms decreases with an increase in Pe and Sb , while the reverse trend is observed with the local Nusselt number of motile microorganisms.

It is anticipated that the present study can be treated as the basis for several engineering and industrial applications. The present article focuses on thermophoresis and Brownian motion effect on MHD flow with Arrhenius activation energy, which can be used in the industrial field for isotope separation, MHD generators, nuclear reactors, and filtration in gas cleaning, and polymer extrusion.

Acknowledgment

We are grateful to the esteemed reviewers for their encouraging comments to improve the original manuscript. One of the authors, Umesh khanduri, is grateful to the Council of Scientific and Industrial Research, New Delhi, for awarding a Junior Research Fellowship.

Declaration of conflicting interests

The authors declared no potential conflicts of interest with respect to the research, authorship, and/or publication of this article.

Funding

The authors received no financial support for the research, authorship, and/or publication of this article.

ORCID iD

Bhupendra Kumar Sharma  <https://orcid.org/0000-0002-2051-9681>

Supplemental material

Supplemental material for this article is available online.

References

1. Crane LJ. Flow past a stretching plate. *Zeitschrift Für Angewandte Mathematik und Physik ZAMP* 1970; 21: 645–647.
2. Gupta PS and Gupta AS. Heat and mass transfer on a stretching sheet with suction or blowing. *Can J Chem Eng* 1977; 55: 744–746.
3. Ali ME. On thermal boundary layer on a power-law stretched surface with suction or injection. *Int J Heat Fluid Flow* 1995; 16: 280–290.
4. Cortell R. Flow and heat transfer of a fluid through a porous medium over a stretching surface with internal heat generation/absorption and suction/blowing. *Fluid Dyn Res* 2005; 37: 231.
5. Ishak A, Nazar R and Pop I. Heat transfer over an unsteady stretching permeable surface with prescribed wall temperature. *Nonlinear Anal: Real World Appl* 2009; 10: 2909–2913.
6. Bhattacharyya K. Effects of radiation and heat source/sink on unsteady MHD boundary layer flow and heat transfer over a shrinking sheet with suction/injection. *Front Chem Sci Eng* 2011; 5: 376–384.
7. Sheikholeslami M, Ganji DD, Javed MY, et al. Effect of thermal radiation on magnetohydrodynamics nanofluid flow and heat transfer by means of two phase model. *J Magn Magn Mater* 2015; 374: 36–43.
8. Kolsi L, Abbasi A, Alqsair UF, et al. Thermal enhancement of ethylene glycol base material with hybrid nanofluid for oblique stagnation point slip flow. *Case Stud Thermal Eng* 2021; 28: 101468.
9. Sharma BK, Gandhi R and Bhatti MM. Entropy analysis of thermally radiating mhd slip flow of hybrid nanoparticles (au-al₂O₃/blood) through a tapered multi-stenosed artery. *Chem Phys Lett* 2022; 790: 139348.
10. Hashemi-Tilehnoee M, Dogonchi AS, Seyyedi SM, et al. Magnetohydrodynamic natural convection and entropy generation analyses inside a nanofluid-filled incinerator-shaped porous cavity with wavy heater block. *J Therm Anal Calorim* 2020; 141: 2033–2045.
11. Hajjar A, Mehryan SAM and Ghalambaz M. Time periodic natural convection heat transfer in a nano-encapsulated phase-change suspension. *Int J Mech Sci* 2020; 166: 105243.
12. Tripathi B and Sharma BK. Effect of heat transfer on MHD blood flow through an inclined stenosed porous artery with variable viscosity and heat source. *Romanian J Biophys* 2018; 28: 89–102.
13. Sharma BK and Kumawat C. Impact of temperature dependent viscosity and thermal conductivity on MHD blood flow through a stretching surface with ohmic effect and chemical reaction. *Nonl Eng* 2021; 10: 255–271.
14. Sharma BK and Gandhi R. Combined effects of joule heating and non-uniform heat source/sink on unsteady mhd mixed convective flow over a vertical stretching surface embedded in a darcy-forchheimer porous medium. *Propul and Power Res* 2022; 11: 276–292.
15. Huang JS, Tsai RY and Huang KH. Numerical study of thermophoresis on aerosol particle deposition from hiemenz flow through porous medium onto a stretching surface. *J Mar Sci Technol* 2012; 20: 163–172.
16. Bai Y, Liu X, Zhang Y, et al. Stagnation-point heat and mass transfer of MHD Maxwell nanofluids over a stretching surface in the presence of thermophoresis. *J Mol Liq* 2016; 224: 1172–1180.
17. Sharma M, Sharma BK, Gaur RK, et al. Soret and dufour effects in biomagnetic fluid of blood flow through a tapered porous stenosed artery. *J Nanofluids* 2019; 8: 327–336.
18. Yazdi MH, Abdullah S, Hashim I, et al. Effects of viscous dissipation on the slip MHD flow and heat transfer past a permeable surface with convective boundary conditions. *Energies* 2011; 4: 2273–2294.

19. Das S, Jana RN and Makinde OD. Magnetohydrodynamic mixed convective slip flow over an inclined porous plate with viscous dissipation and joule heating. *Alexandria Eng J* 2015; 54: 251–261.
20. Haile E and Shankar B. Heat and mass transfer through a porous media of mhd flow of nanofluids with thermal radiation, viscous dissipation and chemical reaction effects. *Am Chem Sci J* 2014; 4: 828–846.
21. Mishra SBKA. Heat source and solet effects on megneto-micropolar fluid flow with variable permeability and chemical reaction. *J Eng Phys Thermophy* 2017; 90: 1488–1499.
22. Tripathi B and Sharma BK. Influence of heat and mass transfer on two-phase blood flow with joule heating and variable viscosity in the presence of variable magnetic field. *Int J Comput Method* 2020; 17: 1850139.
23. Anjalidevi SP and Kandasamy R. Effects of chemical reaction, heat and mass transfer on laminar flow along a semi infinite horizontal plate. *Heat Mass Transf* 1999; 35: 465–467.
24. Afify AA. MHD free convective flow and mass transfer over a stretching sheet with chemical reaction. *Heat Mass Transf* 2004; 40: 495–500.
25. Anki Reddy PB, Reddy SRR and Suneetha S. magnetohydro dynamic flow of blood in a permeable inclined stretching surface with viscous dissipation, non-uniform heat source/sink and chemical reaction. *Front Heat Mass Transfer (FHMT)* 2018; 10(22): 1–10.
26. Pal D and Mondal H. Effects of solet dufour, chemical reaction and thermal radiation on MHD non-darcy unsteady mixed convective heat and mass transfer over a stretching sheet. *Commun Nonlinear Sci Numer Simul* 2011; 16: 1942–1958.
27. Mabood F, Khan WA and Ismail AI Md. MHD stagnation point flow and heat transfer impinging on stretching sheet with chemical reaction and transpiration. *Chem Eng J* 2015; 273: 430–437.
28. Eid MR. Chemical reaction effect on MHD boundary-layer flow of two-phase nanofluid model over an exponentially stretching sheet with a heat generation. *J Mol Liq* 2016; 220: 718–725.
29. Narayana PVS and Babu DH. Numerical study of MHD heat and mass transfer of a jeffrey fluid over a stretching sheet with chemical reaction and thermal radiation. *J Taiwan Inst Chem Eng* 2016; 59: 18–25.
30. Sharma BK, Singh AP, Yadav K, et al. Effects of chemical reaction on magneto-micropolar fluid flow from a radiative surface with variable permeability. *Int J Appl Mech Eng* 2013; 18: 833–851.
31. Kumar Sharma B, Tailor V and Goyal M. Heat source and solet effects on megneto-micropolar fluid flow with variable permeability and chemical reaction. *Glob J Pure Appl Math* 2017; 13: 5195–5212.
32. Tripathi B and Sharma BK. Effect of variable viscosity on MHD inclined arterial blood flow with chemical reaction. *Int J Appl Mech Eng* 2018; 23: 767–785.
33. Kumawat C, Sharma BK, Al-Mdallal QM, et al. Entropy generation for mhd two phase blood flow through a curved permeable artery having variable viscosity with heat and mass transfer. *Int Commun Heat Mass Transf* 2022; 133: 105954.
34. Kooij DM. Über die zersetzung des gasförmigen phosphorwasserstoffs. *Zeitschrift für physikalische Chemie* 1893; 12: 155–161.
35. Logan SR. The origin and status of the arrhenius equation. *J Chem Educ* 1982; 59: 279.
36. Bestman AR. Natural convection boundary layer with suction and mass transfer in a porous medium. *Int J Energy Res* 1990; 14: 389–396.
37. Zeeshan A, Shehzad N and Ellahi R. Analysis of activation energy in couette-poiseuille flow of nanofluid in the presence of chemical reaction and convective boundary conditions. *Results in Physics* 2018; 8: 502–512.
38. Khan MI, Qayyum S, Hayat T, et al. Entropy generation minimization and binary chemical reaction with arrhenius activation energy in MHD radiative flow of nanomaterial. *J Mol Liq* 2018; 259: 274–283.
39. Khan U, Zaib A, Khan I, et al. Activation energy on MHD flow of titanium alloy (ti6Al4V) nanoparticle along with a cross flow and streamwise direction with binary chemical reaction and non-linear radiation: Dual solutions. *J Mater Res Technol* 2020; 9: 188–199.
40. Xu H and Pop I. Mixed convection flow of a nanofluid over a stretching surface with uniform free stream in the presence of both nanoparticles and gyrotactic microorganisms. *Int J Heat Mass Transf* 2014; 75: 610–623.
41. Naz R, Noor M, Shah Z, et al. Entropy generation optimization in MHD pseudoplastic fluid comprising motile microorganisms with stratification effect. *Alexandria Eng J* 2020; 59: 485–496.
42. Mansour MA, Rashad AM, Mallikarjuna B, et al. MHD mixed bioconvection in a square porous cavity filled by gyrotactic microorganisms. *Int J Heat Technol* 2019; 37: 433–445.
43. D'Addona DM, Conte S, Teti R, et al. Feasibility study of using microorganisms as lubricant component in cutting fluids. *Procedia CIRP* 2020; 88: 606–611.
44. Alsaedi A, Khan MI, Farooq M, et al. Magnetohydrodynamic (MHD) stratified bioconvective flow of nanofluid due to gyrotactic microorganisms. *Adv Powder Technol* 2017; 28: 288–298.
45. Tlili I, Ramzan M, Nisa HU, et al. Onset of gyrotactic microorganisms in MHD micropolar nanofluid flow with partial slip and double stratification. *J King Saud Univ-Sci* 2020; 32: 2741–2751.
46. Kotha G, Kolipaula VR, Rao MVS, et al. Internal heat generation on bioconvection of an MHD nanofluid flow due to gyrotactic microorganisms. *Eur Phys J Plus* 2020; 135: 1–19.
47. Khan MI, Alzahrani F and Hobiny A. Heat transport and nonlinear mixed convective nanomaterial slip flow of walter-B fluid containing gyrotactic microorganisms. *Alexandria Eng J* 2020; 59: 1761–1769.
48. Kolsi L, Selimefendigil F, Öztop HF, et al. Impacts of double rotating cylinders on the forced convection of hybrid nanofluid in a bifurcating channel with partly porous layers. *Case Stud Therm Eng* 2021; 26: 101020.
49. Krishna MV, Jyothi K and Chamkha AJ. Heat and mass transfer on MHD flow of second-grade fluid through porous medium over a semi-infinite vertical stretching sheet. *J Porous Media* 2020; 23: 751–765.
50. Nandkeolyar R, Chamkha AJ and et al. A numerical investigation of Hall and radiation effects on MHD three-dimensional casson fluid flow in a porous medium. *J Porous Media* 2021; 24: 15–30.
51. El-dabe NTM and Mostapha DR. MHD peristaltic flow of a walter's B- fluid with mild stenosis through a porous medium in an endoscope. *J Porous Media* 2019; 22: 1109–1130.

52. Krishna MV, Reddy MG and Chamkha AJ. Heat and mass transfer on unsteady MHD flow through an infinite oscillating vertical porous surface. *J Porous Media* 2021; 24: 81–100.
53. Zaib A, Haq RU and Chamkha AJ. mixed convective flow of a casson fluid over a vertical plate in darcy-brinkman porous medium with slips. *J Porous Media* 2021; 24: 1–11.
54. Sangeetha E and De P. Bioconvection in nanofluid flow embedded in non-darcy porous medium with viscous dissipation and ohmic heating. *J Porous Media* 2021; 24: 15–23.
55. Sharma BK, Sharma PK and Chauhan SK. Effect of mhd on unsteady oscillatory couette flow through porous media. *Int J Appl Mech Eng* 2022; 27: 188–202.
56. Kuznetsov AV. The onset of bioconvection in a suspension of gyrotactic microorganisms in a fluid layer of finite depth heated from below. *Int Commun Heat Mass Transf* 2005; 32: 574–582.
57. Prasad PD, Raju CSK, Varma SVK, et al. Cross diffusion and multiple slips on MHD carreau fluid in a suspension of microorganisms over a variable thickness sheet. *J Braz Soc Mech Sci Eng* 2018; 40: 1–13.
58. RamReddy C, Murthy PVS, Chamkha AJ, et al. Soret effect on mixed convection flow in a nanofluid under convective boundary condition. *Int J Heat Mass Transf* 2013; 64: 384–392.
59. Gandhi R, Sharma BK, Kumawat C, et al. Modeling and analysis of magnetic hybrid nanoparticle (au-al 2 o 3/ blood) based drug delivery through a bell-shaped occluded artery with joule heating, viscous dissipation and variable viscosity effects. *Proc Inst Mech Eng, Part E: J Proces Mech Eng* 2022; 236(5): 2024–2043.

Nomenclature

A unsteadiness parameter
 \tilde{C} fluid concentration (unit: mol/m³)

C_p^* specific heat at constant pressure (unit: J/kg·K)
 \tilde{C}_∞ ambient concentration (unit: mol/m³)
 D_B^* Brownian coefficient
 D_τ^* thermal diffusion coefficient
 E_a activation energy (unit: J)
 Ec Eckert number
 g acceleration due to gravity (unit: m/s²)
 Gc solutal Grashof number
 Gr Grashof number
 K permeability parameter
 M magnetic field parameter
 N_b Brownian motion parameter
 Nn_x local Nusselt number of microorganism
 N_t thermophoresis parameter
 Nu_x local Nusselt number
 Pr Prandtl number
 R radiation parameter
 Sc Schmidt number
 Sh_x Sherwood number
 \tilde{T} fluid temperature (unit: K)
 \tilde{T}_∞ ambient temperature (unit: K)
 $\tilde{u}_\tau, \tilde{v}_\tau$ velocity in x-direction and y-direction (unit: m/s)
 α inclination angle (unit: Radians)
 β coefficient of thermal expansion (unit: K⁻¹)
 β^* coefficient of thermal expansion with concentration (unit: K⁻¹)
 γ chemical reaction parameter
 ζ fluid number
 θ non-dimension temperature parameter
 κ thermal conductivity (unit: W/(m · K))
 ν kinematic viscosity (unit: m²/s)
 ϕ non-dimension concentration parameter
 ρ density of the fluid (unit: kg/m³)
 σ electrical conductivity (unit: S/m)